Excited-state thermionic emission in III-antimonides: Low emittance ultrafast photocathodes

Joel A. Berger, B. L. Rickman, T. Li, A. W. Nicholls, and W. Andreas Schroeder

Citation: Applied Physics Letters **101**, 194103 (2012); doi: 10.1063/1.4766350
View online: http://dx.doi.org/10.1063/1.4766350
View Table of Contents: http://scitation.aip.org/content/aip/journal/apl/101/19?ver=pdfcov
Published by the AIP Publishing

Excited-state thermionic emission in III-antimonides: Low emittance ultrafast photocathodes

Joel A. Berger,[1] B. L. Rickman,[1] T. Li,[1] A. W. Nicholls,[2] and W. Andreas Schroeder[1]
[1]*Department of Physics, University of Illinois at Chicago, 845 W. Taylor Street, Chicago, Illinois 60607-7059, USA*
[2]*Research Resources Center, University of Illinois at Chicago, 845 W. Taylor Street, Chicago, Illinois 60607, USA*

(Received 11 September 2012; accepted 23 October 2012; published online 9 November 2012)

The normalized rms transverse emittance of an electron source is shown to be proportional to $\sqrt{m^*}$, where m^* is the effective mass of the state from which the electron is emitted, by direct observation of the transverse momentum distribution for excited-state thermionic emission from two III-V semiconductor photocathodes, GaSb and InSb, together with a control experiment employing two-photon emission from gold. Simulations of the experiment using an extended analytical Gaussian model of electron pulse propagation are in close agreement with the data. © *2012 American Institute of Physics*. [http://dx.doi.org/10.1063/1.4766350]

Sub-nanosecond (ultrafast) pulsed laser-driven electron sources are now being employed in a wide variety of scientific studies: in particular, ultrafast electron diffraction (UED),[1] ultrafast transmission electron microscopy (UEM),[2] and pulsed x-ray free electron lasers.[3] The spatial quality of these sources is often characterized in terms of their normalized transverse rms emittance;[4,5] $\varepsilon_T = \Delta p_x \Delta x/(m_0 c)$, where $\Delta p_x = \sqrt{\langle p_x^2 \rangle}$ is the rms transverse momentum of the source and $\Delta x = \sqrt{\langle x^2 \rangle}$ is its size (cylindrical symmetry assumed), m_0 is the electron rest mass, and c is the speed of light in vacuum. As a reduction in the source size Δx is limited either by the attainable diffraction-limited focusing or by the short-pulse Child's Law (screening of the electron gun's acceleration field),[6] significant improvements in the performance of scientific instruments employing pulsed electron sources through a reduction in their spatial emittance ε_T (and consequent increase in brightness[7]) may only be possible by decreasing the rms transverse momentum Δp_x of the electron source—an intrinsic property of the emission source.[4,5]

In this letter, we show that, at least for thermionic emission, the effective mass m^* of the electronic state from which the electron was emitted affects the rms transverse momentum; that is, the expression for Δp_x developed in Refs. 4 and 5 for thermionic electron emission should be rewritten to read $\sqrt{m^* k_B T_e}$, where T_e is the temperature of the emitting electron distribution and k_B is Boltzmann's constant. Direct observation of the transverse momentum distribution for excited-state thermionic emission (ESTE) from GaSb and InSb, two similar III-V zincblende semiconductors, demonstrates the m^* dependence. A further experiment employing two-photon assisted thermionic emission (2PTE) from gold, for which $m^* = m_0$,[8] confirms the temperature dependence of Δp_x. Simulations of the experiment using our extended analytical Gaussian (AG) model of electron pulse propagation[9] are in close agreement with the data.

Figure 1 depicts the experimental technique used to determine directly the transverse momentum distributions (and hence Δp_x) of the laser-driven electron sources. The primary laser radiation source for the studies is a home-built, diode-pumped, and thermal-lens-shaped femtosecond Yb:KGW oscillator[10] delivering 250 fs duration pulses at 1047 nm and a 63 MHz repetition rate. This 2 W average power laser is frequency doubled in a 3 mm lithium triborate (LBO) crystal with 50% efficiency to yield ~200 fs green pulses at 523 nm (photon energy, $\hbar\omega = 2.37$ eV). Further doubling with a cylindrical focusing geometry in a 7 mm β-barium borate (BBO) crystal yields 261 nm ($\hbar\omega = 4.75$ eV) UV pulses with a duration of ~4 ps (due to the 600 fs/mm group velocity mismatch between the green and the

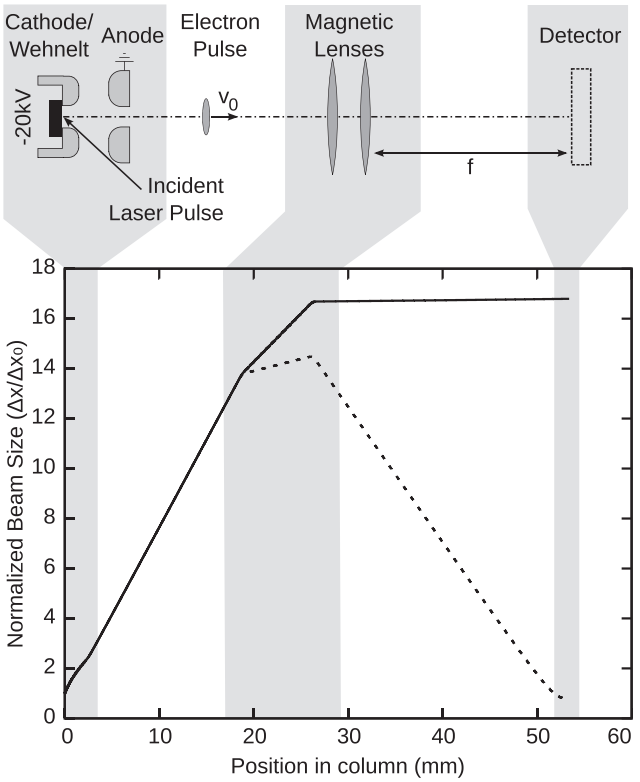

FIG. 1. Schematic of the experiment (top) and simulations of the electron pulse propagation through the apparatus using the extended AG model[9] (bottom). Solid line: The spatial beam width (normalized to that at the photocathode Δx_0) with the magnetic lens strengths adjusted to ensure that the detector is at their back focal plane (Fourier plane). Dashed line: The case when the strength of the magnetic lenses is increased by a factor of two to focus the electron beam on the YAG scintillator detector.

generated UV). Both the green and the UV laser pulses are focused with 30 cm focal lenses onto the photocathode in a 20 kV electron gun at an angle of incidence of $60(\pm 5)^\circ$, which improves the coupling of the *p*-polarized laser radiation into the photocathode surface.[7] The electron gun design is based on that of Togawa *et al.*[7,11] and has an acceleration gap of $25(\pm 2)$ mm. After acceleration in the dc photo-gun, the electrons pass through a set of electrostatic deflection plates to ensure that the electron beam passes, as close as possible, axially through the center of two, 6.35-mm-bore, thin and round magnetic lenses with counter-propagating currents to minimize image rotation effects. A YAG scintillator placed 27.5 cm after the second magnetic lens detects the spatial electron beam profile, and its visible fluorescence is 1:1 imaged onto a CCD detector with 5.4 μm pixels.

To ensure that the transverse momentum distribution is observed, the YAG scintillator must be positioned at the back focal plane (the Fourier plane) of the lens system. This is readily achieved by appropriate adjustment of the current I in the magnetic lens coils; specifically, after determining the current required to focus the electron beam onto the scintillator, optical imaging relations together with the I^2 dependence of the magnetic lens strength are used to find the current that ensures that the average lens to scintillator distance equals the focal length of the lens system. Simulation of the experimental apparatus, also shown in Figure 1, confirms that this procedure places the YAG scintillator at the back focal plane of the lens system to within a ± 0.5 cm error. This simulation, which employs the extended AG model for electron pulse propagation,[9] also confirms that for our experimental conditions (less than 5000 electrons/pulse and $\Delta x > 30$ μm) space-charge effects do not influence the observations. Additionally, and as expected from optical considerations, the modeling shows that the spatial beam size in the Fourier plane is independent of the incident laser spot size on the photocathode (i.e., the electron source size, Δx_0).

To verify the efficacy of the experimental technique, we monitored the momentum distribution (Fourier plane spot size) for electrons emitted by 2PTE from gold using the ~200 fs green (523 nm) *p*-polarized laser pulses. Due to the 60° angle of incidence, the circular laser beam is focused by the 30 cm focal length lens to an elliptical 50×100 μm (half-width 1/e maximum ($HWe^{-1}M$) of the field) spot size on the photocathode surface. The results, the measured Fourier plane beam size and electron yield, are displayed in Figure 2 as a function of the incident laser pulse energy, corrected to account for 10% optical loss (mainly from the uncoated vacuum system windows).

The quadratic dependence of the electron yield on pulse energy clearly indicates a two-photon emission process. This is expected since an excitation energy of two green photons ($\hbar\omega = 2.37$ eV) will be required to overcome the reported $\phi = 4.69$ eV effective work function of a thick gold film contaminated with adsorbed water[12] or ensure that at least the tail of the electron Fermi distribution has sufficient energy to overcome the $5.1(\pm 0.1)$ eV work function of a clean Au surface.[13] Moreover, when $2\hbar\omega \approx \phi$, the dependence of the yield on the square of the electron's excess energy above the work function[12] ensures that predominantly only the high energy (Boltzmann) tail of the Fermi distribution contributes to the emission. Consequently, the observed increase in Δp_x with incident pulse energy must be due to a heating effect; specifically, laser heating of the free electron Fermi gas as two-photon excitation is instantaneous and the ~200 fs green laser pulse duration excludes any coupling to the lattice which occurs on the time scale of a few picoseconds.[14] The solid line in Figure 2 is the predicted variation derived using a simple zero free parameter model of this effect. Using the known optical properties of gold,[8] which give a reflectance $R_p = 0.53$ and an absorption depth of 20 nm, and the temperature-dependent heat capacity of a free electron Fermi gas, the model evaluates the *average* temperature of the laser-heated electron gas that may be two-photon excited assuming that only electrons within a few nanometers of the surface can be emitted, as the mean free path for electrons in Au is ~4 nm.[15] This average electron temperature T_e is then used in the AG model simulation of the experiment (Figure 1) to determine the expected Fourier plane spot size on the YAG scintillator, that is, using an initial $\Delta p_x = \sqrt{m_0 k_B T_e}$. The dashed lines indicate the expected trends for a $\pm 10\%$ error in the laser spot size Δx_0 incident on the gold cathode surface. The close agreement between the data and the simulation strongly supports our interpretation of the emission mechanism and, as expected, that the effective mass of a free electron in Au is equal to the rest mass m_0.[8]

Figure 3 depicts the results obtained for GaSb and InSb photocathode materials under pulsed UV (261 nm) laser irradiation using the same experimental technique. Both samples are cut from [100]-oriented polished wafers; the GaSb is undoped and the InSb is moderately *p*-type. Prior studies[16] indicate that single-photon photoemission should not possible for either semiconductor—the effective photoemission work functions (about 4.8 eV for undoped GaSb and 4.89 eV for *p*-type InSb (Fermi level pinned at valence band maximum)) being greater than the 4.75 eV photon energy even when the 34 meV Schottky barrier suppression due to the

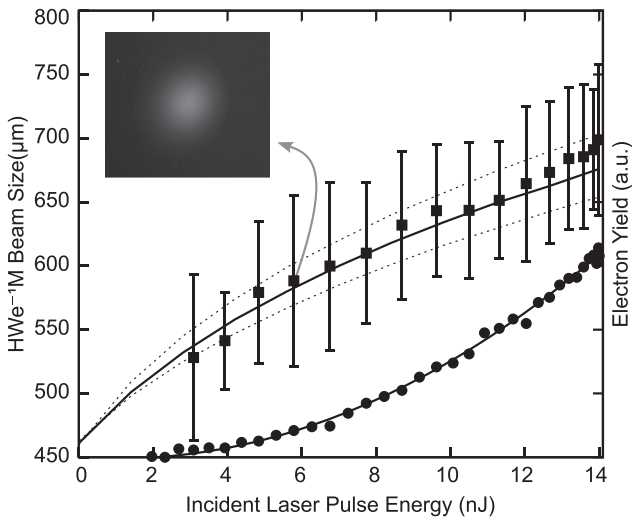

FIG. 2. Measured Fourier plane electron beam size ($HWe^{-1}M$; squares) and electron yield (circles) as a function of the incident ~200 fs, 523 nm laser pulse energy for the 300-nm-thick gold photocathode. The electron yield is proportional to the square of laser pulse energy (solid line) and the dependence of the beam size with the laser pulse energy fits that is predicted by a zero free parameter electron heating model (solid line; dashed lines represent $\pm 10\%$ error in the laser spot size). A representative raw Fourier plane beam image is also shown.

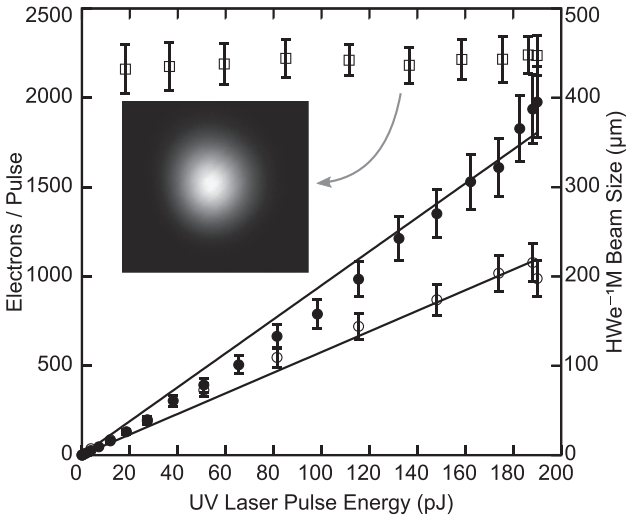

FIG. 3. Number of electrons emitted per pulse as a function of the incident 261 nm, UV laser pulse energy for GaSb (open squares) and InSb (filled circles): Linear efficiency dependences are shown by the solid lines. The laser pulse energy invariance of the Fourier plane electron beam size ($HWe^{-1}M$ right axis; open squares) for GaSb and a representative raw Fourier plane beam image is also shown.

applied 8 kV/cm dc field is included.[4] Nonetheless, for both zincblende semiconductors, significant laser-driven emission (more than expected for a single-photon field emission process) is observed with a yield nearly linearly proportional to the ~4 ps UV laser pulse energy.

The known optical properties of the two semiconductors[17] indicate that a strong absorption at 261 nm, with an optical absorption depth of only 7-8 nm, which, based on the band structures of GaSb[18] and InSb,[19] is primarily due to promotion of electrons near the Γ point from the valence band (heavy-hole, light-hole, and split-off bands) directly into the upper Γ_8 conduction band located at 3.77 eV and 3.59 eV above the valence band maximum in GaSb and InSb, respectively. Assuming parabolic bands and an estimated effective mass m^* of about $0.3\,m_0$ ($0.5\,m_0$) for the Γ_8 conduction band in GaSb (InSb), we determine that these electrons are excited with an average excess energy (above the Γ_8 conduction band minimum) of ~0.35 eV (~0.41 eV). For the ~0.1 nJ incident UV pulse energies, ~40 μm laser spot size, and *p*-polarized reflectance of ~40% for both semiconductors at our 60° incidence angle, the photoinjected electron density is $\sim 10^{18}\,cm^{-3}$. At these carrier densities, which are non-degenerate for the upper Γ_8 conduction bands, we expect rapid thermalization[20] and, consequently, an electron distribution with a well-populated Boltzmann tail extending above the vacuum level located at an effective work function ϕ of 0.99 eV (1.18 eV) above the Γ_8 conduction band minimum in GaSb (InSb); thus allowing for thermionic emission from this excited state as initially $\exp[-\phi/(k_B T_e)] \approx 0.06$ in both semiconductors.

Carrier cooling, primarily by longitudinal optical (LO) phonon emission, and decay out of the upper conduction band to lower states will rapidly deplete the Boltzmann tail above ϕ, thereby curtailing the observed ESTE. By comparison with the Γ_6 conduction band Fröhlich coupling constant in GaAs, where the characteristic LO phonon emission time is 165 fs for a hot electron in the Γ_6 conduction band,[21] we estimate that hot electrons in the upper Γ_8 conduction band of both GaSb and InSb emit a LO phonon every ~200 fs with an energy of 29 and 24 meV, respectively. This means that even without population decay mechanisms the temperature of the exited electron distribution T_e drops at a rate of ~1600 K/ps in both semiconductors. We note that the close proximity of the lower and unconfined (in momentum space) Γ_7 upper conduction band to the Γ_8 band will likely result in a fast population decay so that the observed ESTE process should have an intrinsic latency of much less than the ~4 ps UV laser pulse duration.

Figure 3 also shows that the measured Fourier plane electron beam spot size for GaSb is independent of the UV laser pulse energy, as would be expected for the proposed emission process. More significantly, using $\Delta p_x = \sqrt{m_0 k_B T_e}$ (i.e., assuming that the emitted electrons have a mass m_0 in the semiconductor), simulation of the experiment with the extended AG model[9] indicates that the observed GaSb Fourier plane spot size of 0.45(±0.03) mm ($HWe^{-1}M$) would be due to an electron temperature $T_e \approx 360$ K, which is associated with negligible thermionic emission ($\exp[-\phi/(k_B T_e)] \sim 10^{-15}$). On the other hand, employing a mass of $0.3\,m_0$ for the electrons in GaSb allows an average electron temperature (over the ~4 ps laser pulse duration) of about 1200 K to be extracted using the AG model simulation—a value much more consistent with the proposed ESTE mechanism and the expected cooling rate by LO phonon emission. In fact, at the maximum ~0.2 nJ incident UV laser pulse energy up to 10^8 electrons/pulse could be excited into the upper Γ_8 conduction band, of which one in $\exp[\phi/(k_B T_e)] \approx 20\,000$ is above the effective 0.99 eV work function, thus agreeing with the observed yield of $\sim 10^3$ electrons/pulse (Figure 3). We also note that the normalized transverse rms emittance ε_T of this UV laser-driven ultrafast GaSb electron source is more than a factor of two less than that expected from a *standard* Cu photocathode ($\phi = 4.31$ eV and assuming $\Delta p_x = \sqrt{m_0(\hbar\omega - \varphi)/3}$, where $\hbar\omega$ is the incident photon energy[4,5]) irradiated at the same 261 nm wavelength.

Very similar results are observed with the *p*-type InSb photocathode except that the Fourier plane spot size is 30%–40% larger and the electron yield is a factor of 1.7 higher. The increased rms transverse momentum for the same ESTE process is consistent with the larger $\sim 0.5 m_0$ effective mass of the upper Γ_8 conduction band in InSb, the expected higher initial temperature of the electron distribution, and the marginally slower cooling process associated with the lower 24 meV LO phonon energy. The resultant higher average electron temperature T_e also contributes to the increased electron yield that is likely further enhanced by a larger absorption into the upper Γ_8 conduction band (due to its larger effective mass) and a 4% lower *p*-polarized reflectance for the 60° incident UV laser radiation.[17]

The dependence of Δp_x on m^* is readily explained through a consideration of energy and momentum conservation in transmission across a boundary with a potential step associated with the effective photoelectric work function ϕ. Inside the material, an electron with an energy E greater than ϕ has a maximum momentum of $\sqrt{2m^*(E-\phi)}$ parallel to the boundary if it is to be emitted. As this momentum component is conserved in emission from the material surface into

the vacuum, the rms transverse momentum Δp_x of the electron source clearly must scale with $\sqrt{m^*}$ as observed in the experiment. This is, of course, the *sine qua non* of angle-resolved photoemission studies[22] where determination of the electron emission angle and energy allows the effective mass parallel to the sample surface to be determined. We note that the electron effective mass also causes the narrow emission cone reported for *p*-type GaAs(100) negative electron affinity photocathodes,[23] where surface cesiation lowers the vacuum level below the Γ_6-valley minimum ($m^* = 0.067\, m_0$) to allow for direct emission of electrons excited into the conduction band. For direct single-photon photoemission, we would therefore also expect to require that the expression describing the rms transverse momentum to be written as $\Delta p_x = \sqrt{m^*(\hbar\omega - \phi)/3}$. Efforts are currently underway to determine if this is indeed the case using a variety of metal photocathodes and the ~4 ps, 261 nm laser radiation source.

This work was supported by the Department of Energy (Contract DE-FG52-09NA29451) and J.A.B. acknowledges the support of a Department of Education GAANN fellowship (Contract DED P200A070409).

[1]G. Scianini and R. J. D. Miller, "Femtosecond electron diffraction: Heralding the era of atomically resolved dynamics," Rep. Prog. Phys. **74**, 096101 (2011).
[2]W. E. King, G. H. Campbell, A. Frank, B. Reed, J. F. Schmerge, B. J. Siwick, B. C. Stuart, and P. M. Weber, "Ultrafast electron microscopy in materials science, biology, and chemistry," J. Appl. Phys. **97**, 111101 (2005).
[3]D. H. Dowell, I. Bazarov, B. Dunham, K. Harkay, C. Hernandez-Garcia, R. Legg, H. Padmore, T. Rao, J. Smedley, and W. Wan, "Cathode R&D for future light sources," Nucl. Instrum. Methods Phys. Res. A **622**, 685–697 (2010).
[4]D. H. Dowell and J. F. Schmerge, "The quantum efficiency and thermal emittance of metal photocathodes," Phys. Rev. ST Accel. Beams **12**, 074201 (2009).
[5]K. L. Jensen, P. G. O'Shea, D. W. Feldman, and J. L. Shaw, "Emittance of a field emission electron source," J. Appl. Phys. **107**, 014903 (2010).
[6]A. Valfells, D. W. Feldman, M. Virgo, P. G. O'Shea, and Y. Y. Lau, "Effects of pulse-length and emitter area on virtual cathode formation in electron guns," Phys. Plasmas **9**, 2377–2382 (2002).
[7]J. A. Berger, J. T. Hogan, M. J. Greco, W. A. Schroeder, A. W. Nicholls, and N. D. Browning, "DC photoelectron gun parameters for ultrafast electron microscopy," Microsc. Microanal. **15**, 298–313 (2009).
[8]P. B. Johnson and R. W. Christy, "Optical constants of the noble metals," Phys. Rev. B **6**, 4370–4379 (1972).
[9]J. A. Berger and W. A. Schroeder, "Semi-analytic model of electron pulse propagation: Magnetic lenses and RF pulse compression cavities," J. Appl. Phys. **108**, 124905 (2010).
[10]J. A. Berger, M. J. Greco, and W. A. Schroeder, "High-power, femtosecond, thermal-lens-shaped Yb:KGW oscillator," Opt. Express **16**, 8629–8640 (2008).
[11]K. Togawa, T. Shintake, T. Inagaki, K. Onoe, and T. Tanaka, "CeB_6 electron gun for low-emittance injector," Phys. Rev. ST Accel. Beams **10**, 020703 (2007).
[12]H. Monjushiro, I. Watanabe, and Y. Yokoyama, "Ultraviolet electron yield spectra of thin gold films measured in air," Anal. Sci. **7**, 543–547 (1991).
[13]D. E. Eastman, "Photoelectric work functions of transition, rare-earth, and noble metals," Phys. Rev. B **2**, 1–2 (1970).
[14]J. K. Chen, D. Y. Tzou, and J. E. Beraun, "A semiclassical two-temperature model for ultrafast laser heating," Int. J. Heat Mass Transfer **49**, 307–316 (2006).
[15]M. P. Seah and W. A. Dench, "Quantitative electron spectroscopy of surfaces: A standard data base for electron mean free paths in solids," Surf. Interface Anal. **1**, 2–11 (1979).
[16]G. W. Gobeli and F. G. Allen, "Photoelectric properties of cleaved GaAs, GaSb, InAs, and InSb surfaces; comparison with Si and Ge," Phys. Rev. **137**, A245–A254 (1965).
[17]D. E. Aspnes and A. A. Studna, "Dielectric functions and optical parameters of Si, Ge, GaP, GaAs, GaSb, InP, InAs, and InSb from 1.5 to 6.0 eV," Phys. Rev. B **27**, 985–1009 (1983).
[18]J. R. Chelikowsky and M. L. Cohen, "Nonlocal pseudopotential calculations for the electronic structure of eleven diamond and zinc-blende semiconductors," Phys. Rev. B **14**, 556 (1976).
[19]J. R. Chelikowsky and M. L. Cohen, "Erratum: Nonlocal pseudopotential calculations for the electronic structure of eleven diamond and zinc-blende semiconductors [Phys. Rev. B 14, 556 (1976)]," Phys. Rev. B **30**, 4828 (1984).
[20]M. T. Portella, J.-Y. Bigot, R. W. Schoenlein, J. E. Cunningham, and C. V. Shank, "k-space carrier dynamics in GaAs," Appl. Phys. Lett. **60**, 2123–2125 (1992).
[21]J. A. Kash, J. C. Tsang, and J. M. Hvam, "Subpicosecond time-resolved Raman spectroscopy of LO phonons in GaAs," Phys. Rev. Lett. **54**, 2151–2154 (1985).
[22]F. J. Himpsel, "Angle-resolved measurements of the photoemission of electrons in the study of solids," Adv. Phys. **32**, 1–51 (1983).
[23]Z. Liu, Y. Sun, P. Pianetta, and R. F. W. Pease, "Narrow cone emission from negative electron affinity photocathodes," J. Vac. Sci. Technol. B **23**, 2758–2762 (2005).